Journal of Catalysis **190,** 419–432 (2000)
doi:10.1006/jcat.1999.2761, available online at http://www.idealibrary.com on IDEAL®

Hydroisomerization of Heptane Isomers over Pd/SAPO Molecular Sieves: Influence of the Acid and Metal Site Concentration and the Transport Properties on the Activity and Selectivity

M. Höchtl,* A. Jentys,† and H. Vinek*,[1]

*Institute of Physical and Theoretical Chemistry, Vienna University of Technology, Getreidemarkt 9/156, A-1060 Vienna, Austria; and †Institute of Technical Chemistry II, Technical University of Münich, Lichtenbergstr. 4, D-85748 Garching, Germany

Received August 6, 1999; revised November 16, 1999; accepted November 18, 1999

The hydroconversion of *n*-heptane and heptane isomers over Pd/SAPO-5 and Pd/SAPO-11 was studied. The Pd/SAPO-11 catalysts differed in concentration of the acid sites but not in the acid strength. At a given acid site concentration, the activity increased until a Pd/acid site ratio of 0.03 was reached; further improvement in activity and selectivity was obtained with increasing acid site concentration. The diffusion coefficients obtained by time-resolved infrared measurements decreased in the sequence *n*-heptane ≈ 2-methylhexane > 3-methylhexane for SAPO-11 and *n*-heptane ≈ 2-methylhexane > 3-methylhexane > 2,4-dimethylpentane > 2,3-dimethylpentane > 2,2,3-trimethylbutane for SAPO-5. The difference in the diffusion coefficients was reflected in the different reactivities and in the product distribution of the heptane isomers. The higher reactivity of the dibranched isomers compensated their lower diffusivity over the wider pore SAPO-5. The pores of SAPO-11 were only partially accessible for multibranched isomers under reaction conditions. In the *n*-heptane conversion over hybrid catalysts (mixed HSAPO-11 and Pd/SiO_2) the same activities and selectivities compared to those of Pd/SAPO-11 were found, indicating that the distance between acid and metal sites has only a minor influence as long as the supported metal and the SAPO phase are in direct contact.

Key Words: **hydroisomerization; SAPO; metal/acid sites; mechanism.**

INTRODUCTION

Platinum or palladium supported on microporous silico–aluminum phosphates are highly efficient catalysts for the hydroisomerization of long chain alkanes. The hydroconversion of *n*-heptane over Pd- or Pt-containing SAPO molecular sieves was extensively studied in the past few years (1–4) and a high selectivity for the formation of monomethylhexanes over SAPO-11 and of mono- and multibranched isomers with a tendency to cracking over SAPO-5 was reported (2).

[1] To whom correspondence should be addressed. Fax: +43/1/25077/3816. E-mail: vinek@tuwien.ac.at.

The conversion of linear into monobranched alkanes plays an important role in dewaxing of paraffinic feedstock (5). The preferential formation of terminal monobranched alkanes in 10-membered ring systems like the $AlPO_4$-11 structure results from restricted transition-state (6–8) or product-shape selectivity (8). These selectivities are due to the spatial restriction of pore dimensions on the formation of bulkier intermediates or on the motion of bulkier product molecules within the structure. The complete exclusion of bulky reactant molecules is unlikely; however, their rate of disappearance or the rate of formation of a product molecule will be rather low but not zero.

The product distribution of hydroisomerization is determined by the average lifetime of the carbocation intermediates, which depends on the acid site density, metal–acid site ratio, and acid strength. Furthermore, the pore structure and the crystallite size have a crucial influence on the catalytic performance of hydroisomerization catalysts (9). Small changes in either the pore diameter or the molecular size can change the diffusivity of alkanes by orders of magnitude (10).

The hydroconversion of *n*-alkanes over bifunctional catalysts is supposed to proceed via a bifunctional mechanism as suggested by Weisz *et al.* (11). In the first step the *n*-alkane is dehydrogenated on the metal sites; subsequently, the alkene is isomerized and can undergo β-scission on the acid site. In the final reaction step the products are hydrogenated and desorbed as saturated hydrocarbons. In principle, this mechanism is generally accepted, but some modifications have been made. S. Tiong Sie introduced the protonated cyclopropane (PCP) structure as intermediate for isomerization and cracking (12–14) on the acid sites, which according to the reaction scheme proposed, occur as parallel reactions.

Chu *et al.* (15) proposed an acid-catalyzed chain reaction with the only role of the metal to hydrogenate alkenes. The metal and acid sites should be as near as possible to prevent an increase in the local concentration of alkenes.

0021-9517/00 $35.00

Other explanations suggest that hydrogen adsorbed on metal particles serves as a hydride donor and reacts with the isomerized carbenium ion to form product molecules (16). Zhang *et al.* (17), studying the hydroisomerization of *n*-pentane, proposed a hydrogen spillover from the metal particle to the zeolites as H^+ and H^- ions. A direct interaction of the metal and the protonic sites of the acidic support material by the formation of a metal–proton adduct, acting as an active site for hydrocarbon rearrangement, is discussed in (18).

The main objective of the present work was to determine the activity and selectivity in hydroisomerization of *n*-heptane and heptane isomers over Pd/SAPO-5 and Pd/SAPO-11. The influence of the concentration of acid and metal sites and the diffusivities of the different heptane isomers on the reaction mechanism was investigated.

EXPERIMENTAL

Synthesis

The silico–aluminum phosphates were synthesized according to the patent literature (19). Orthophosphoric acid and 30% Silica-Sol (Merck) were used as phosphorus and silicon sources, respectively. SAPO-5 was prepared using pseudoboehmit (Condea Pural NG, 170 m^2/g) and triethylamine (Aldrich) as templating agents.

The synthesis of the SAPO-11 molecular sieves is described in (20). Two series of samples were prepared using aluminumisopropoxide (Aldrich) (SAPO-11/1,2) or pseudoboehmit (SAPO-11/3-6) as the aluminum source and di-*n*-propylamine as the templating agent.

$AlPO_4$-11 was synthesized according to a method by Tapp *et al.* (21), using pseudoboehmit. After the as-synthesized molecular sieves were washed and dried, the template was removed at 600°C in dry air. The structures of the as-synthesized and the calcined samples were proved by X-ray diffraction using a Seifert ID3000 diffractometer.

Catalysts containing 0.1–2 wt% palladium were prepared by the incipient wetness method. $Pd(NH_3)_4Cl_2 \cdot H_2O$, dissolved in an appropriate quantity of distilled water to fill the pores of the molecular sieve, was added dropwise to the dry sample while stirring. After impregnation, the samples were slowly heated to 70°C and finally dried at 110°C. The metal precursor was decomposed in flowing oxygen at 450°C and subsequently the metal was reduced in hydrogen at the same temperature.

Hybrid catalysts were prepared by mechanically mixing Pd-impregnated SiO_2 and calcined SAPO-11/4. This catalyst was used in the manually mixed form or compressed with 1 t/cm^2 pressure and subsequently crushed in a mortar.

Reference data for the zero concentration of strong acid sites were obtained from Pd/$AlPO_4$-11.

Characterization

Energy-dispersive X-ray analysis (EDX) was used to determine the chemical composition of the samples. The BET surface area was calculated from N_2 adsorption isotherms at 77 K. Scanning electron microscope measurements (SEM) were carried out to describe the morphology and to estimate the particle size of the materials. The palladium dispersion was determined from hydrogen adsorption isotherms measured in a volumetric adsorption apparatus (22, 23).

Temperature-programmed desorption (TPD) of ammonia was used to determine the number of strong acid sites. Ammonia (1 mbar) was adsorbed at room temperature, evacuated to 10^{-3} mbar, and desorbed with a heating rate of 10°C min^{-1}.

The infrared (ir) spectra were recorded in transmission mode on a Bruker IFS 28 spectrometer with a resolution of 4 cm^{-1}. The calcined samples were pressed into self-supporting wavers that were placed inside a ring furnace in a vacuum cell. The samples were activated at 500°C and a pressure $<2 \times 10^{-6}$ mbar for 1 h and then cooled to 40°C. *n*-Heptane (*n*-C_7), 2-methylhexane (2-MC_6), 3-methylhexane (3-MC_6), 2,4-dimethylpentane (2,4-DMC_5), 2,3-dimethylpentane (2,3-DMC_5), and 2,2,3-trimethylbutane (2,2,3-TMC_4) were adsorbed in a pressure range from 10^{-3} to 20 mbar. For the determination of the diffusion coefficients, 15 spectra were accumulated every 10 s at 10^{-3} mbar hydrocarbon pressure, until the equilibrium was reached.

The time-resolved ir spectra were recorded every 10 s during the adsorption of 10^{-3} mbar *n*-heptane. A series of heptane isomers with increasing kinetic diameters ranging from 0.43 nm (*n*-heptane) to 0.62 nm (2,2,3-trimethylbutane) (24) was used to determine the accessibility and the molecular transport to the acid sites. The integrated area of the C–H stretching vibrations was taken as the measure for the amount of hydrocarbon adsorbed. The diffusion coefficients were estimated by applying the solution of Fick's law for spherical or cubic particles (10, 25):

$$\frac{M_t}{M_\infty} = \frac{6}{r\sqrt{\pi}}\sqrt{Dt}.$$

M_t/M_∞ represents the fractional hydrocarbon uptake at time t and at equilibrium. For the calculation of the diffusion coefficient the slope of the linear part of the plot M_t/M_∞ vs $t^{1/2}$ ($0.2 < M_t/M_\infty < 0.6$) was used (Fig. 1).

Kinetic Experiments

The hydroconversion of heptane was measured in a microreactor system using a quartz glass reactor with 4-mm inner diameter typically containing between 5 and 20 mg of the catalyst that was diluted with the same mass of quartz sand. The hydrocarbons were introduced into the hydrogen carrier gas stream by a saturator or syringe pump to obtain a partial pressure of 25 mbar at a total pressure of

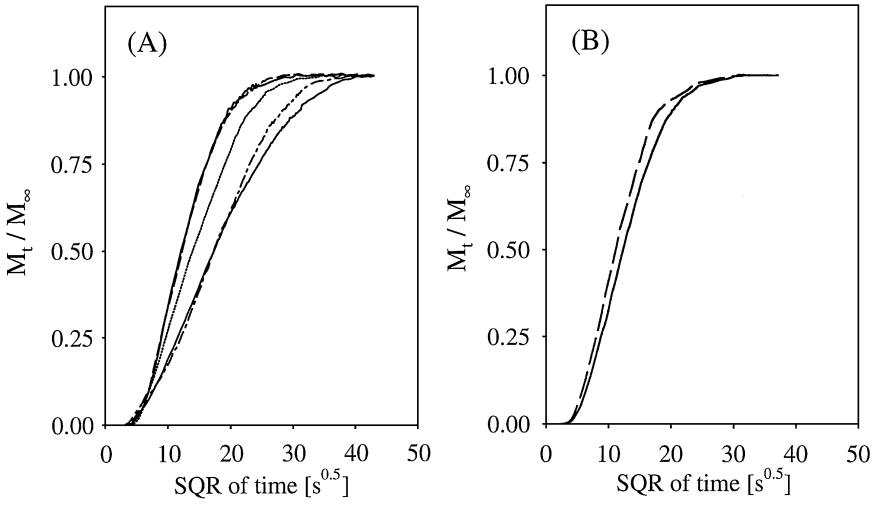

FIG. 1. Integrated area of the CH stretching vibrations vs square root of time during the C_7 adsorption on (A) SAPO-5 and (B) SAPO-11: $p = 10^{-3}$ mbar; $T = 40°C$. ———, n-C_7; — — —, 2-MC_6; ·····, 2,4-DMC_5; —·—, 2,3-DMC_5; ▬▬ 2,2,3-TMC_4.

3 bar and a gas flow between 3 and 100 cm^3/min. The hydrocarbon conversion was measured at temperatures between 225 and 450°C. The Pd loading was 1 wt% for all kinetic experiments unless otherwise mentioned.

To investigate the influence of the distance between acid and metal sites, the acid and the metal component of the catalysts were separated by positioning layers of palladium impregnated on SiO_2 and SAPO-11 separated by quartz wool layers of the desired length in the reactor.

The reaction products were analyzed by a GC using a 60-m × 0.25-mm HP-5 high-resolution column and a FID. The kinetic data were collected at conversions below 10% and the rates were calculated from the rate expression for differential conditions.

RESULTS

Characterization

Table 1 summarizes the composition, the concentration of acid sites, the BET surface area, and the mean particle size of the calcined molecular sieves. The structures of all materials were confirmed by XRD. The concentration of strong Brønsted acid sites was in the range between 0.09 and 0.3 mmol/g. The acid strength, deduced from NH_3-TPD and ir-spectroscopic investigations after adsorption of benzene, did not depend on the composition for SAPO-11, while it was found to be slightly lower for SAPO-5 (20).

The SEM picture from $AlPO_4$-11 exhibited prisms and plates with a length between 1 and 5 μm (Fig. 2a). For the SAPO-11 series synthesized with pseudoboehmit (Fig. 2b) an inhomogeneous particle size distribution was observed. The crystals were in the shape of prisms and plates with a diameter between 1 and 5 μm, but did not show larger agglomerates or oligocrystalline intergrowth. In contrast, SAPO-11 synthesized with aluminum isopropoxide exhibited polycrystalline spheres with a diameter of 10–20 μm which consisted of prisms and needles with a length of 2–6 μm (Fig. 2c). Similarly, SAPO-5 (Fig. 2d) showed spheres with a diameter between 4 and 8 μm and smaller needle-shaped crystals.

The dispersion of palladium on the different SAPO-11 samples and on SAPO-5 is compared in Table 2. At a metal loading of 1% or higher, the dispersion was always below 10%, while for the samples 0.1 wt% Pd on SAPO-11 the dispersion was between 30 and 40%.

In the ir spectra of activated SAPO molecular sieves five OH bands were observed (23, 26), i.e., terminal Al–OH (3800 cm^{-1}), Si–OH (3740 cm^{-1}), and P–OH (3676 cm^{-1}), bridged SiAl–OH (3628 cm^{-1}), and internal interacting SiAl–OH groups (3520 cm^{-1}).

In Fig. 3 the difference spectra of the O–H and C–H stretching vibrations after the adsorption of n-C_7, 2-MC_6,

TABLE 1

Chemical and Physical Properties of SAPO-11 and SAPO-5 Samples

	Al (mol%)	P (mol%)	Si (mol%)	Brønsted acid sites[c] (mmol/g)	BET (m^2/g)	Mean particle size (μm)
SAPO-11/1[a]	49.7	49.4	0.9	0.09	154	3.5
SAPO-11/2[a]	48.8	49.1	2.1	0.24	202	4
SAPO-11/3[b]	61.0	36.6	2.4	0.19	174	2
SAPO-11/4[b]	52.2	44.9	2.9	0.23	184	3
SAPO-11/5[b]	51.2	45.6	3.2	0.29	180	3.5
SAPO-11/6[b]	48.6	48.7	2.7	0.30	182	2.5
SAPO-5[b]	45.6	45.9	8.5	0.24	339	5

[a] SAPO-11 synthesized from pseudoboehmit.
[b] SAPO-11 synthesized from aluminum isopropoxide.
[c] Determined by NH_3-TPD.

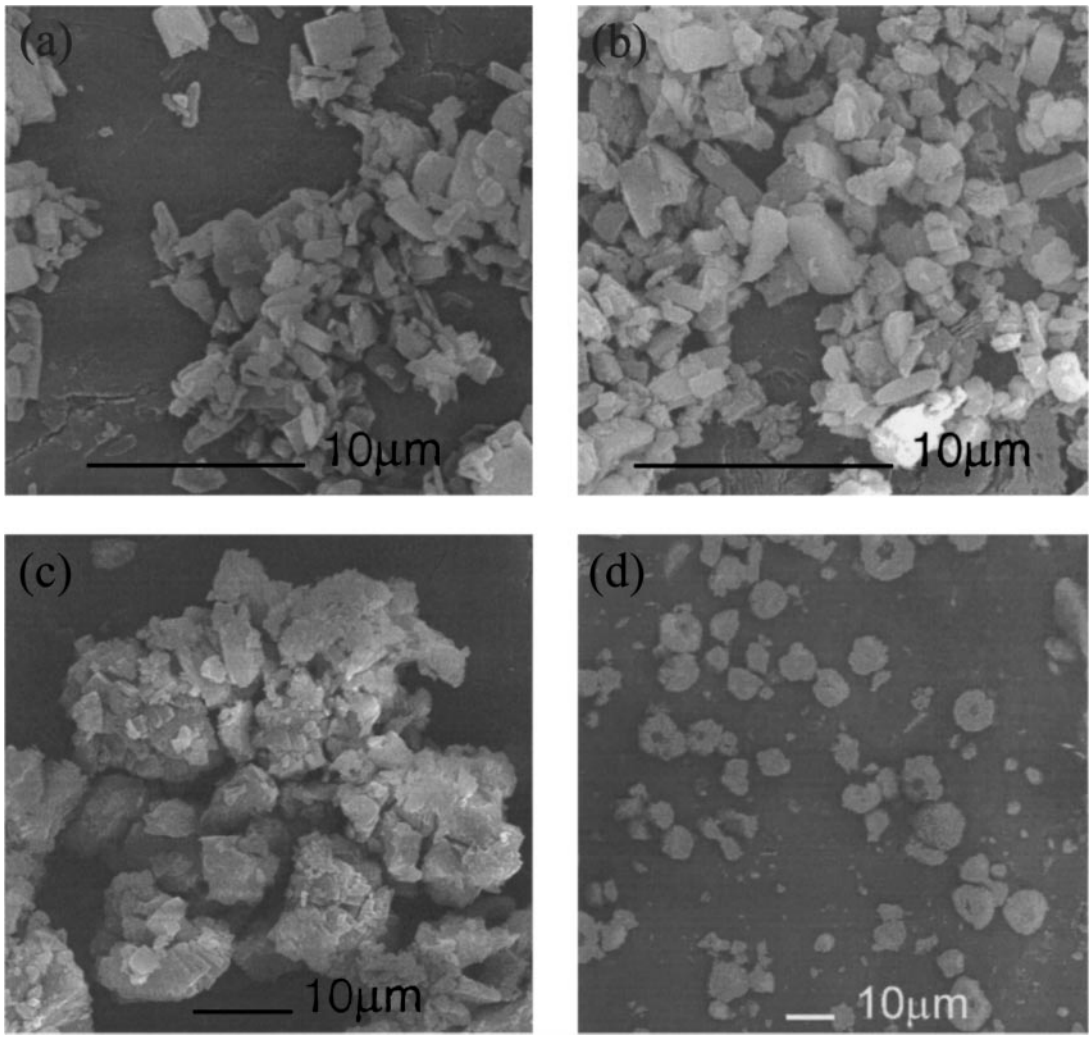

FIG. 2. Scanning electron micrographs of (a) $AlPO_4$-11, (b) SAPO-11/4, (c) SAPO-11/2, and (d) SAPO-5.

TABLE 2

Dispersion and Metal-to-Acid Site Ratios of Pd/SAPO-11 and Pd/SAPO-5

	Pd loading (wt%)	Dispersion (%)	Pd/H ratio
SAPO-11/1	1	7	0.073
SAPO-11/2	1	8	0.033
SAPO-11/3	0.1	39	0.019
SAPO-11/3	0.25	17.5	0.021
SAPO-11/3	0.5	10.5	0.026
SAPO-11/3	1	8	0.039
SAPO-11/3	2	7	0.069
SAPO-11/4	0.1	33	0.013
SAPO-11/4	0.25	15.5	0.015
SAPO-11/4	0.5	10	0.021
SAPO-11/4	1	8	0.033
SAPO-11/4	2	7	0.057
SAPO-11/5	1	8	0.026
SAPO-11/6	1	9	0.028
SAPO-5	1	7	0.029

2,3- and 2,4-DMC_5, and 2,2,3-TMC_4 on SAPO-11/4 are shown. At an equilibrium pressure of 10^{-3} mbar (Fig. 3A), a decrease of the band at 3628 cm^{-1} indicated an interaction of *n*-C_7 and 2-MC_6 with bridged hydroxyl groups. The resulting shift of the OH stretching vibration gave rise to bands at 3505 cm^{-1} (*n*-C_7) and 3495 cm^{-1} (2-MC_6). To a small extent 2,3- and 2,4-DMC_5 was adsorbed on the bridged hydroxyls (SiAl–OH), whereas no interaction was observed for 2,2,3-TMC_4.

After equilibration with 2,2,3-TMC_4 at 1 mbar, a decrease of the bands at 3740, 3678, and 3628 cm^{-1} was detected (Fig. 3B). However, the decrease of the SiAl–OH band was only 5% compared to the adsorption of *n*-C_7 or 2-MC_6, suggesting that this fraction of the bridged acid sites is located near the pore openings. 2,3-DMC_5 could access 20% of the acid sites accessible for *n*-C_7 and 2-MC_6; thus, there was clear evidence that dimethyl-branched probe molecules could enter the pores of SAPO-11 molecular sieves. The shifted band of perturbed SiAl–OH groups after adsorption of 2,3-DMC_5 appeared at 3490 cm^{-1}.

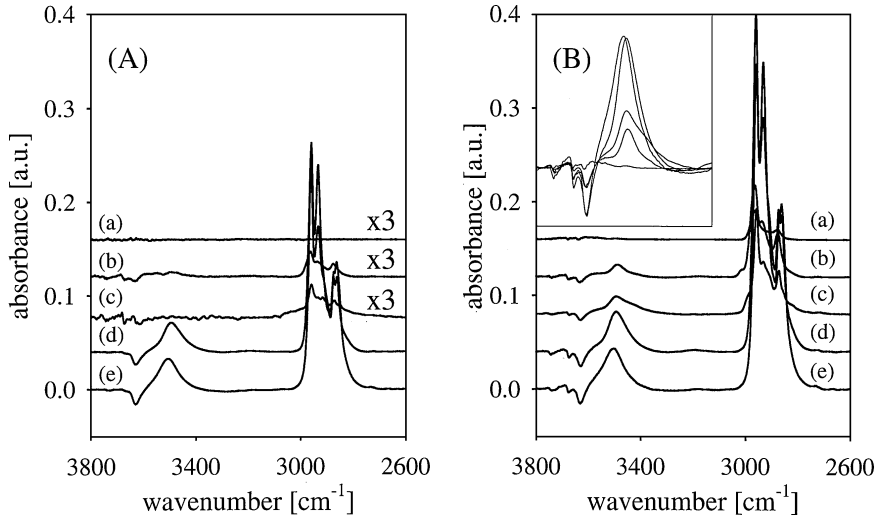

FIG. 3. ir spectra of the OH and CH stretching region after adsorption of (a) 2,2,3-TMC_4, (b) 2,3-DMC_5, (c) 2,4-DMC_5, (d) 2-MC_6, and (e) n-C_7, at an equilibrium pressure of 10^{-3} mbar (A) and 1 mbar (B).

On SAPO-5 practically all acid sites were accessible for the heptane isomers, as expected from the larger pore diameter of the AFI framework.

The diffusion coefficients, the diffusivity relative to n-C_7, and the normalized area of the C–H stretching vibrations relative to n-C_7 are depicted in Table 3. On SAPO-5 the diffusivities decreased, in general, with the degree of branching, showing almost identical values for n-C_7 and 2-MC_6 and an even higher value for 2-MC_6 on SAPO-11. The diffusivity of 3-MC_6 was lower than that for 2-MC_6 on both molecular sieves. The diffusion coefficients of multibranched isomers in SAPO-11 could not be calculated as no significant uptake was observed under the adsorption conditions.

Kinetic Measurements

In all experiments, the catalysts generally deactivated slightly during the first 10 min of the reaction; afterward, the activity became stable.

The selectivities and the conversion rates of C_7 compounds over 1 wt% Pd/SAPO-5 and Pd/SAPO-11/4 at 300°C are presented in Tables 4 and 5. The selectivities in Tables 5a and 5b are calculated relative to the sum of C_7 products.

The selectivity to isomerization and to cracked products and the total conversion rate are shown in Figs. 4 and 5. Generally, in the larger pore SAPO-5 catalyst (Fig. 4) the formation of dibranched isomers was more favored than in the smaller pores of SAPO-11 (Fig. 5). Dibranched molecules as the reactant yielded 5 and 15% of n-heptane over SAPO-11 while SAPO-5 showed only a n-C_7 selectivity of 0.3%.

The apparent activation energies measured between 250 and 325°C and a heptane conversion around 5% are given in Table 6. n-C_7 and 2-MC_6 showed the same apparent activation energy, i.e., 115 ± 5 kJ/mol over SAPO-11 and 135 ± 6 kJ/mol over SAPO-5, indicating no diffusion limitation for the 2-methyl isomer. However, the activation energy decreased with increasing diameter of the molecules and the low values observed for the reaction of 2,2,3-TMC_4, i.e., 21 and 8 kJ/mol for SAPO-5 and SAPO-11, respectively, indicated a significant diffusion limitation.

TABLE 3

Diffusion Coefficients and C–H-Stretching-Vibration Area (Relative to n-C_7)

	SAPO-5,			SAPO-11,		
	Area (n-C_7 = 1)	$D \times 10^{10}$ (cm^2/s)	D_{rel} (n-C_7 = 1)	Area (n-C_7 = 1)	$D \times 10^{10}$ (cm^2/s)	D_{rel} (n-C_7 = 1)
n-C_7	1	1.16	1	1	0.38	1
2-MC_6	0.97	1.12	0.97	0.46	0.45	1.18
3-MC_6	0.88	0.88	0.76	0.16	0.32	0.84
2,4-DMC_5	0.85	0.68	0.59	0.02	—	
2,3-DMC_5	0.88	0.46	0.39	0.01	—	
2,2,3-TMC_4	0.83	0.38	0.33	0.00	—	

TABLE 4a

Activity, Selectivity (%), and Iso/*n*-C_4 Ratio of the C_7 Hydroconversion over 1 wt% Pd/SAPO-5: $T = 300^\circ$C; $p = 3$ bar; Conversions < 10%

	SAPO-5					
	n-C_7	2-MC_6	3-MC_6	2,4-DMC_5	2,3-DMC_5	2,2,3-TMC_4
Total rate (mol $g^{-1} s^{-1}$)	2.0×10^{-7}	7.7×10^{-7}	1.0×10^{-6}	1.2×10^{-6}	1.9×10^{-6}	1.5×10^{-7}
C_1–C_6	6.3	4.2	8.3	8.1	11.0	20.4
n-C_7	—	3.8	5.3	0.3	0.3	1.1
MC_6	87.9	71.0	74.4	11.8	14.7	11.6
$DMC_5 + TMC_4$	5.8	21.0	12.0	79.8	74.0	66.9
Iso/*n*-C_4	9.5	1.12	1.8	13.3	20.9	9.9

Hydroconversion of n-C_7

Isomerization was the main reaction with 2-MC_6 and 3-MC_6 as primary products over SAPO-5 and SAPO-11. Only small amounts of 2,3- and 2,4-DMC_5 were detected over SAPO-11. Over SAPO-5 additionally 2,2-DMC_5, 3,3-DMC_5, and 3-ethylpentane were found. At higher temperatures the selectivity to dibranched isomers and hydrocracking increased. Note that the iso/*n*-butane ratio was below 1 over SAPO-11 and below 10 over SAPO-5 (Tables 4a and 4b). The order of the *n*-heptane reaction over 1% Pd/SAPO-11 was –0.4 in hydrogen and 0.7 in *n*-C_7. Increasing the hydrogen pressure resulted in an increasing selectivity to monobranched isomers, while the selectivities to dibranched isomers and cracking decreased.

Hydroconversion of 2-MC_6 and 3-MC_6

3-Methylhexane was the main product of the 2-MC_6 hydroconversion with a selectivity around 70% over SAPO-5 and 60% over SAPO-11 at 300°C. Other products were *n*-C_7 over SAPO-11 and dibranched isomers over SAPO-5. The selectivity to dibranched isomers was 4.3% over SAPO-11 and 21% over SAPO-5, while the selectivity for *n*-heptane was higher on SAPO-11 (24.5%) compared to SAPO-5 (3.8%). The rate of the 2-MC_6 conversion was about the same on both molecular sieves and higher than the conversion rate of *n*-heptane.

The level of the 3-MC_6 conversion was close to that of 2-MC_6. On SAPO-11 the lower diffusivity caused a decrease in the total rate compared to the conversion of 2-MC_6. The methyl shift to 2-MC_6 was the preferred reaction of 3-MC_6 over both types of molecular sieves with a selectivity of 73% on SAPO-11 and 66% on SAPO-5. Over SAPO-5 3-ethylpentane was formed with a selectivity around 15%, while only lower amounts of dibranched isomers were found.

Hydroconversion of 2,3-DMC_5 and 2,4-DMC_5

On both catalysts the main reaction was the 1,2-methyl shift from 2,3- to 2,4-dimethylpentane and vice versa. Over SAPO-5 the amount of dibranched isomers was much higher compared to SAPO-11 and 2,2- and 3,3-DMC_5 were detected as additional primary products. With increasing conversion, the selectivity to dibranched isomers decreased, while the formation of 2- and 3-MC_6 increased and that of 3,3-DMC_5 was constant. The steric restrictions of the SAPO-11 pores led to a much lower activity for the 2,3- and

TABLE 4b

Activity, Selectivity (%), and Iso/*n*-C_4 Ratio of the C_7 Hydroconversion over 1 wt% Pd/SAPO-11: $T = 300^\circ$C; $p = 3$ bar; Conversion < 10%

	SAPO-11				
	n-C_7	2-MC_6	3-MC_6	2,4-DMC_5	2,3-DMC_5
Total rate (mol $g^{-1} s^{-1}$)	3.5×10^{-7}	6.9×10^{-7}	5.8×10^{-7}	1.1×10^{-7}	1.1×10^{-7}
C_1–C_6	5.8	3.6	5.1	10.6	5.1
n-C_7	—	31.3	22.4	13.7	4.2
MC_6	93.2	59.7	69.5	30.6	40.4
$DMC_5 + TMC_4$	1.0	5.4	3.1	45.1	50.3
Iso/*n*-C_4	0.5	0.6	0.8	2.7	2.4

TABLE 5a

Isomerization Selectivity (%) of the C_7 Hydroconversion over 1 wt% Pd/SAPO-5: $T = 300^\circ$C; $p = 3$ bar; Conversion < 10%

	SAPO-5					
	n-C_7	2-MC_6	3-MC_6	2,4-DMC_5	2,3-DMC_5	2,2,3-TMC_4
n-C_7	—	3.9	5.3	0.3	0.3	1.4
2-MC_6	42.5	—	65.7	7.4	7.1	6.7
3-MC_6	48.0	70.7	—	5.1	8.5	6.9
3-EC_5	3.3	3.4	16.2	0.3	0.9	1.0
2,2-DMC_5	0.9	0.7	1.2	9.9	29.6	7.6
2,3-DMC_5	3.2	18.1	8.5	69.8	—	30.0
2,4-DMC_5	1.7	2.7	2.2	—	33.6	42.1
3,3-DMC_5	0.4	0.5	0.8	5.9	19.6	4.3
2,2,3-TMC_4			0.1	1.3	0.4	—

TABLE 5b

Selectivity (%) to C_7 Isomers of the C_7 Hydroconversion over 1 wt% Pd/SAPO-11: $T = 300°C$; $p = 3$ bar; Conversion < 10%

	SAPO-11					
	n-C_7	2-MC_6	3-MC_6	2,4-DMC_5	2,3-DMC_5	Equilibrium (27)
n-C_7		32.5	23.7	15.4	4.4	14.0
2-MC_6	60.6		73.0	23.7	28.4	23.2
3-MC_6	38.3	61.9		10.8	14.2	27.4
3-EC_5						3.1
2,2-DMC_5				0.8	2.3	7.8
2,3-DMC_5	0.7	4.1	2.6	48.7		10.9
2,4-DMC_5	0.4	1.5	0.7		49.2	7.2
3,3-DMC_5				0.6	1.5	4.7
2,2,3-TMC_4						1.7

2,4-DMC_5 conversion compared to SAPO-5. Furthermore, the influence of the smaller pore size of SAPO-11 was reflected in a lower selectivity to dibranched isomers. However, the high selectivity to the formation of monobranched isomers compared to that of SAPO-5, i.e., mainly 2-MC_6, suggested that the reaction occurred inside the pores. Over SAPO-11 and SAPO-5 the 2,4-DMC_5 and 2,3-DMC_5 exhibited almost the same total rate, being 1 order of magnitude higher over that of SAPO-5.

Hydroconversion 2,2,3-TMC_4

As shown by ir spectroscopy, the pores of SAPO-11 were completely inaccessible for 2,2,3-TMC_4. Therefore, the rate observed was 2 orders of magnitude lower than that for n-C_7.

Over SAPO-5, the rate of 2,2,3-TMC_4 conversion was comparable to that of the n-C_7 conversion. The main products were dibranched C_7 isomers, with higher yields of 2,3-DMC_5 and of the thermodynamically unfavorable 2,4-DMC_5, indicating a transport limitation for the bulkier 2,2- and 3,3-DMC_5. Monobranched isomers and products from cracking reactions were detected only in small concentrations.

Influence of the Acid Site Concentration

In Fig. 6 the activity and selectivity as functions of the concentration of strong Brønsted acid sites on Pd/SAPO-11 of the n-heptane and 2,3-DMC_5 hydroconversion are shown. Both the activity and the isomerization selectivity increased with increasing number of acid sites. The n-C_7 isomerization selectivity was above 90% except for those of $AlPO_4$-11 and the SAPO-11 samples with the lowest silicon content and was unaffected by the acid site density above 0.2 mmol/g. SAPO-11/2 (synthesized from an aluminum isopropoxide

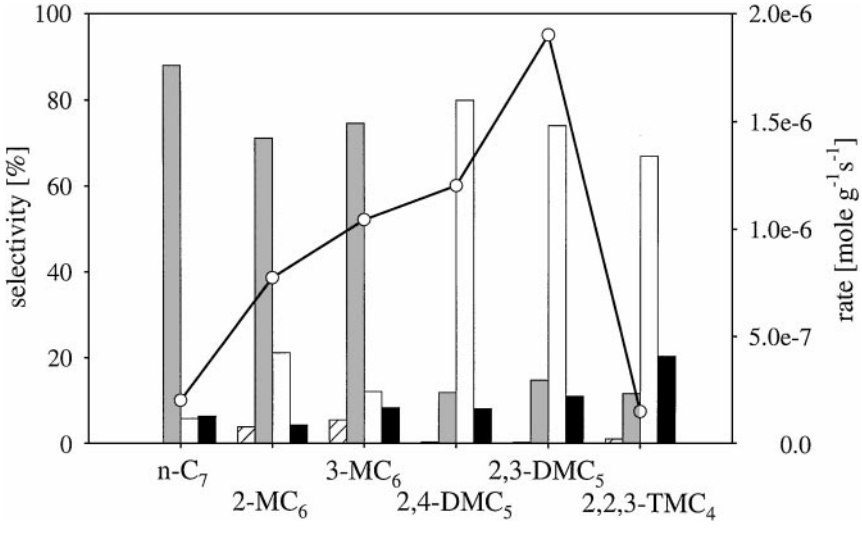

FIG. 4. Selectivities and total rate of the hydroconversion of different C_7 isomers over 1 wt% Pd/SAPO-5: $T = 300°C$; $p = 3$ bar; $p_{C_7} = 25$ mbar; total conversion < 10%. ▨, n-C_7; ▬, M-C_6; □, $DMC_5 + TMC_4$; ■, C_1–C_6; —○—, total rate (mol g^{-1} s^{-1}).

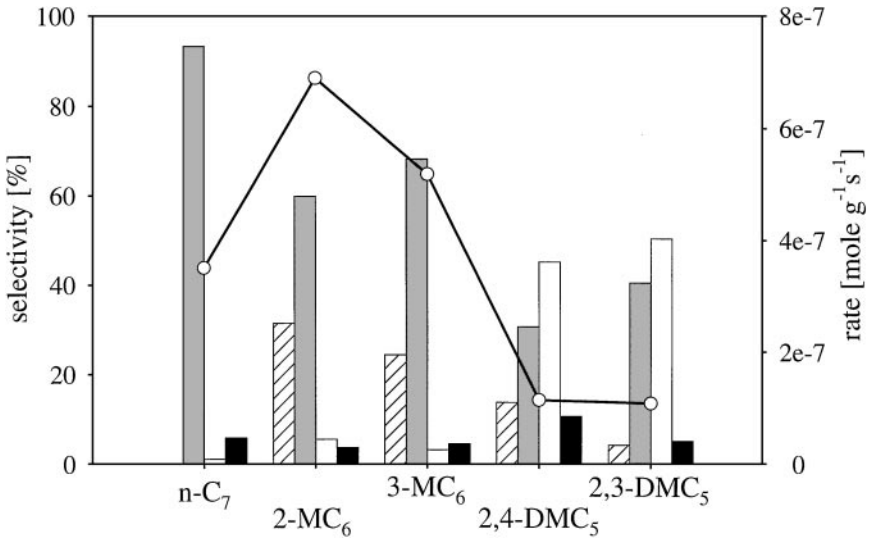

FIG. 5. Selectivities and total rate of the hydroconversion of different C_7 isomers over 1 wt% Pd/SAPO-11/4: $T = 300°C$; $p = 3$ bar; $p_{C_7} = 25$ mbar; total conversion < 10%. ▨, *n*-C_7; ▬, *M*-C_6; □, $DMC_5 + TMC_4$; ■, C_1–C_6; —○—, total rate (mol g^{-1} s^{-1}).

gel) exhibited a lower activity compared to the Al_2O_3-synthesized samples with a similar acid site concentration. The activity for the 2,3-DMC_5 reaction also increased with increasing number of strong acid sites on the SAPO-11 catalysts, confirming that the molecule reacted inside the pores.

Influence of the Metal/Acid Site Ratio

The effect of different metal/acid site ratios on the activity is presented in Fig. 7 for SAPO-11 catalysts with different acid site concentrations. The total rate reached a plateau between a Pd/H ratio of 0.02 and 0.03 for all catalysts studied (see Fig. 7, gray area).

To investigate the influence of the metal siting relative to the acid sites on the activity and selectivity in hydroisomerization, the impregnated samples were compared to hybrid catalysts. In Fig. 8 the selectivity and the activity of differently prepared Pd/SAPO-11/4 catalysts are shown. The data presented were measured at 300°C and a total pressure of 3 bar. The metal-to-acid site ratio of the hybrid catalysts corresponded to that of the impregnated SAPO-11.

Sample (A) was an impregnated Pd/SAPO-11 catalyst, while (B) was a compressed catalyst and (C) a mechanically mixed hybrid catalyst. The activity and the selectivity of the hybrid catalyst (B) toward isomerization were comparable to those of the impregnated catalyst (A). The mechanically mixed hybrid catalyst (C) exhibited a slightly lower selectivity and practically the same rate as the impregnated SAPO-11.

The complete separation of the metal and acid sites into two layers Pd/SiO_2//SAPO-11 (D) resulted in a loss of the synergetic effect of acid and metal sites, which was reflected in a product selectivity close to that of Pd/SiO_2 (E) accompanied by a strong decrease of the total rate. Additionally, the results for the *n*-C_7 conversion over $Pd/AlPO_4$-11 are given (F). Over catalysts (D)–(F) additional reaction products such as cyclic and aromatic C_7 and traces of unsaturated compounds were found (Fig. 8, black column areas).

It should be noted that the total rate of the *n*-C_7 hydroconversion over 1% $Pd/AlPO_4$-11 was 1×10^{-8} mol s^{-1} g^{-1} and over Pd/SiO_2 4×10^{-9} mol s^{-1} g^{-1}. SAPO-11/4 without Pd exhibited under the same reaction conditions solely cracking with a rate below 1×10^{-9} mol s^{-1} g^{-1}.

TABLE 6

Activation Energies for the Conversion of Different C_7 Isomers

Catalyst	$E_{a(app.)}$(kJ mol^{-1})					
	n-C_7	2-MC_6	3-MC_6	2,4-DMC_5	2,3-DMC_5	2,2,3-TMC_4
Pd/SAPO-5	135	135	120	131	91	21
Pd/SAPO-11	115	115	90	80	75	8

DISCUSSION

To optimize hydroisomerization, catalysts with a well-balanced ratio between acid and metal sites are required. Moreover, the geometry and the dimensions of the catalyst pores should suppress hydrocracking to improve the yield of isomerization.

On SAPO molecular sieves the presence of various types of hydroxyl groups was reported (26, 28). Among those, the bridged SiAl–OH hydroxyl groups are supposed to be the catalytically most active acid sites for hydroisomerization. The acid strength of these sites was found to be higher on SAPO-11 than on SAPO-5, as proven by NH_3-TPD and the

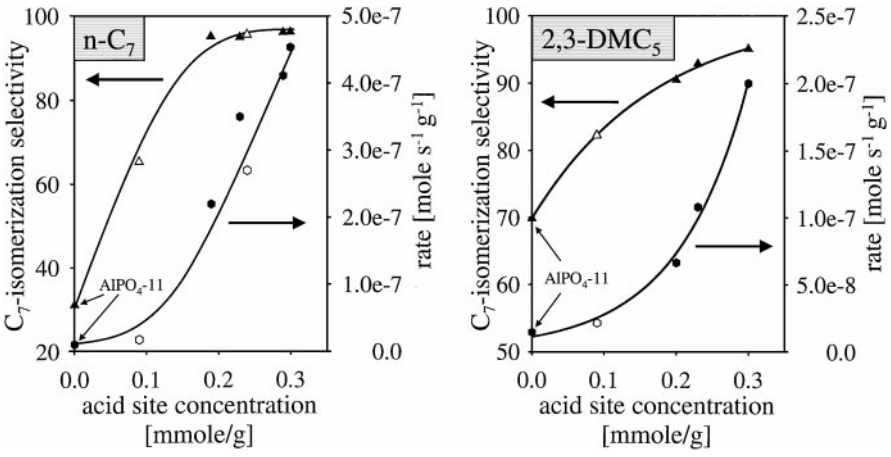

FIG. 6. Dependence of the total rate (●) and the selectivity (▲) of n-C_7 and 2,3-DMC_5 on the acid site concentration of 1 wt% Pd/SAPO-11 synthesized from Al_2O_3 (black marks) and aluminium isopropoxide (white marks): $T = 300°C$; $p = 3$ bar; $p_{C_7} = 25$ mbar; total conversion <10%.

interaction with benzene (23). It was shown that Pd-loaded $AlPO_4$-11 exhibited an activity and product selectivity similar to Pd impregnated on fumed silica (Fig. 8F), indicating that P–OH groups do not posses sufficient acid strength to catalyze this reaction.

Diffusivity and Accessibility

The monodimensional pore system of SAPO-11 consists of nonintersecting elliptical 10-membered ring pores with 0.39- × 0.63-nm diameters (29). SAPO-5 has one-dimensional pores with a larger diameter (0.73 nm). n-C_7, 2- and 3-MC_6, 2,3- and 2,4-DMC_5, and to a minor extent 2,2,3-TMC_4 should be able to diffuse into the pores of SAPO-5, whereas in the narrow pores of SAPO-11 strong diffusional limitations should exist for the dibranched isomers. It is even clearer that 2,2,3-TMC_4 with a kinetic diameter larger than 0.62 could hardly enter the channels of SAPO-11 and hence would react only with the acid sites present on the external surface of the crystals. However, adsorption and diffusion measurements at pressures of 10^{-1} mbar and higher indicated that all molecules except 2,2,3-TMC_4 have access at least to a part of the acid sites of SAPO-11 at 40°C. Considering the higher mobility of the dibranched C_7 molecules at reaction conditions, it seems therefore to be very likely that they may react on the acid sites located inside the catalyst particles.

The diffusion coefficient derived from time-resolved ir measurements confirmed that no diffusion limitations exist for n-C_7 and 2-MC_6 in both molecular sieves and that severe limitations for 2,3- and 2,4-DMC_5 and 2,2,3-TMC_4 in SAPO-11 are present. In a comparison of data for diffusion coefficients in microporous systems reported in the literature, differences in the order of magnitudes can be found (30). Therefore, a diffusion coefficient relative to n-C_7 is given (Table 3). Note that the relative diffusion

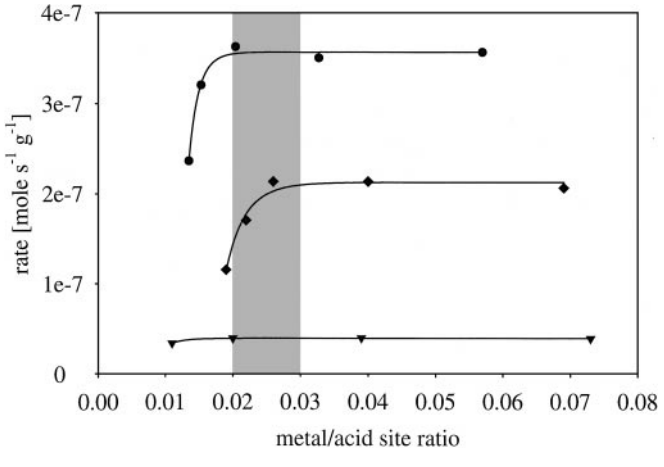

FIG. 7. Activity of Pd/SAPO-11/1 (▼), Pd/SAPO-11/3 (◆), and Pd/SAPO-11/4 (●) impregnated with 0.1–2 wt% palladium for the n-C_7 hydroconversion: $T = 300°C$; $p = 3$ bar; $p_{C_7} = 25$ mbar.

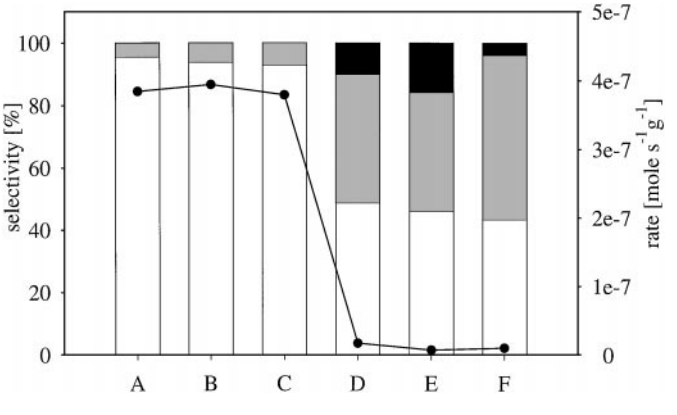

FIG. 8. Influence of the metal–acid site distance on the n-C_7 hydroconversion: $T = 300°C$; $p = 3$ bar; $p_{C_7} = 25$ mbar; 1 wt% Pd loading. □, C_7 isomers; ▨, C_1–C_6; ■, other C_7; —●—, total rate (mol g^{-1} s^{-1}). (A) Impregnated Pd/SAPO-11; (B) Pd/SiO_2–SAPO-11 hybrid catalyst, compressed; (C) Pd/SiO_2–SAPO-11 hybrid catalyst, mixed; (D) Pd/SiO_2–SAPO-11 layers; (E) Pd/SiO_2; (F) Pd/$AlPO_4$-11.

coefficient for 2-MC_6 in SAPO-11 is even slightly higher than that of *n*-C_7. This is in contrast to diffusion measurements in other 10-membered molecular sieves such as HZSM-5 (10). The AEL structure possesses 6-membered ring openings to small side pockets in the channel wall. Probably, the interaction of the methyl group with the center of these rings is energetically favorable. Diffusion down the channel can be accomplished by jumps between successive pocket mouths (31).

Acid and Metal Sites

Impregnation with typically 1% palladium led to the formation of particles with dispersions lower than 10%. The Pd-particle sizes estimated from the metal dispersion was between 15 and 30 nm, suggesting that the particles were too large to fit into the SAPO pores. Therefore, the main part of the metal must be located on the outer surface of the SAPO crystals. It was shown by adsorption measurements that the metal deposition did not affect the accessibility of the acid sites (32).

Increasing the Pd content led to an increase of the conversion and the isomerization selectivity until a plateau was reached at a metal/acid sites ratio of about 0.02–0.03 (Fig. 7). This is in agreement with the results of Guisnet *et al.* (33), who found an increase of the hydroisomerization/hydrocracking activity up to a metal-to-acid site ratio of 0.03 over various platinum-loaded zeolites.

Further enhancement of the reaction rate is only possible by a higher concentration of acid sites (Fig. 6). For the conversion of *n*-C_7 and 2,3-DMC_5 it was shown that the isomerization selectivity increased with an increasing concentration of acid sites, indicating that the hydroconversion activity and selectivity of the different Pd/SAPO samples must be essentially a result of the acidic properties.

Metal Loading and Distance

The metal in a bifunctional catalyst is considered to produce unsaturated hydrocarbon intermediates. Secondly, the metal activates hydrogen that is required for the hydrogenation of the cracked or isomerized intermediates on the surface. The metal and acid sites therefore ought to be in close vicinity (15, 34). A metal–proton adduct as suggested in (18), which requires a close proximity of the metal and acid sites, can be excluded due to the large metal particles, which are not likely located inside the pores.

Zhang *et al.* (17) found a comparable activity and an even better selectivity in the reaction of *n*-alkanes over mechanically mixed Pt/SiO_2–HZSM-5 hybrid catalysts than over Pt supported on HZSM-5. They explained the role of the metal by hydrogen spillover, where protons, generated by heterolytic scission of H_2 on the Pt sites, act as acids and abstract a hydride ion from the hydrocarbon molecule to form a carbenium ion. It was shown by these results that even inhomogeneous mixtures of Pd/SiO_2 with HZSM-5 exhibited synergistic effects typical of bifunctional catalysts, which is in accordance with the results presented for Pd/SiO_2–SAPO-11 hybrid catalysts. For different mechanical mixtures of Pd/SiO_2 and SAPO-11 almost the same results in activity and selectivity were found as those for impregnated SAPO-11, indicating that the distance between the acid and metal sites has only a minor influence as long as the supported metal and the SAPO are in direct contact.

Additionally, spilled over hydrogen is responsible for the enhancement of the alkane desorption from the acid sites. Therefore, an increasing hydrogen concentration could increase not only the desorption of isomerized products before they undergo cracking but also the desorption of unreacted molecules. The negative order in hydrogen can be explained by the shift in the alkane/alkene equilibrium (35); however, it could also be caused by the spillover hydrogen-promoted desorption of reactant molecules. Hence, it may be concluded that unsaturated intermediates as well as spilled over hydrogen are involved in the hydrocarbon reaction over bifunctional catalysts.

The complete separation of the catalyst layers led to a loss of activity and isomerization selectivity. Due to the low activity of SAPO-11 without palladium, hydrocarbon conversion occurred solely on the metal, which is reflected in the product selectivities. There was no evidence of gas-phase spilled over hydrogen, as described in the literature (36, 37). This was confirmed by ir spectroscopy during H/D exchange of an impregnated sample, a hybrid catalyst, and a sample that consisted of a Pd/SiO_2 and a SAPO-11 wafer, separated by a SiO_2 disc. The presence of *in situ* reduced palladium accelerated the H/D exchange of the acid sites compared to that of pure SAPO-11. The hybrid catalysts exhibited an H/D exchange rate close to that of the impregnated catalyst, while the acid sites separated from the D_2 activating metal showed, like SAPO-11, a significantly slower exchange activity (38).

Activity and Selectivity for Heptane Conversions

Significant differences in the activities of the different heptane isomers were observed over SAPO-11 and SAPO-5 catalysts (Figs. 4 and 5). The different pore dimensions of SAPO-5 and SAPO-11, reflected in the diffusion coefficients, caused differences in the residence times of the reaction intermediates in the channels and therefore in the product distribution. The reaction schemes for C_7 isomerization over SAPO-11 and SAPO-5 are shown in Figs. 9A and 9B. The isomerization rates for the primary reactions are related to the rate for *n*-C_7 to 2-MC_6 over SAPO-5, which is arbitrarily set to 100. The fastest reaction over SAPO-11 is the 1,2-methyl shift from 2-MC_6 to 3-MC_6 (and vice versa), whereas the methyl shift in the dibranched isomers is very slow, due to the minor reactivity of dibranched isomers in SAPO-11. Over SAPO-5 the

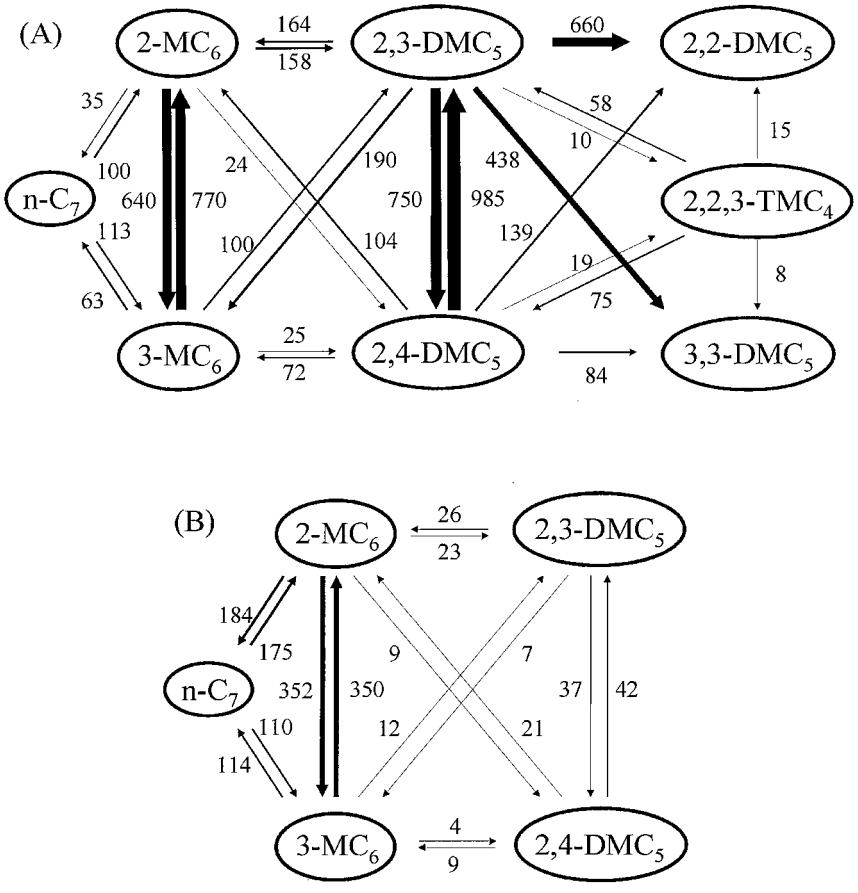

FIG. 9. Reaction scheme of various C_7 isomers over SAPO-5 (A) and SAPO-11 (B). The values represent the rates multiplied with the selectivities to primary products. The reaction of n-C_7 to 2-MC_6 over SAPO-5 is set to 100.

1,2-methyl shift in the dibranched and monobranched isomers are the most preferred reaction pathways.

Conversion of n-Heptane

Under the reaction conditions chosen ($T \leq 300$°C, 5% total conversion), SAPO-11 showed a higher activity for the n-C_7 conversion than SAPO-5. The activation energies are close to the values reported by Campelo *et al.* (1). In the temperature range from 225 to 300°C the average values for the apparent E_a were 115 kJ/mol for SAPO-11 and 135 kJ/mol for SAPO-5. Eder (39) measured the adsorption enthalpies of various alkanes on $AlPO_4$-5 and $AlPO_4$-11 and found a difference of about 20 kJ/mol with the higher absolute value for $AlPO_4$-11. Thus, the sum of adsorption enthalpy and apparent activation energy (~200 kJ/mol) is about the same for n-heptane over SAPO-5 and SAPO-11.

Figure 10 shows the Arrhenius plots between 250 and 450°C. While the apparent activation energy derived for the n-heptane conversion over SAPO-5 was constant within the given temperature range, a decrease to 50 kJ/mol over SAPO-11 above 300°C was observed, indicating mass transport limitations.

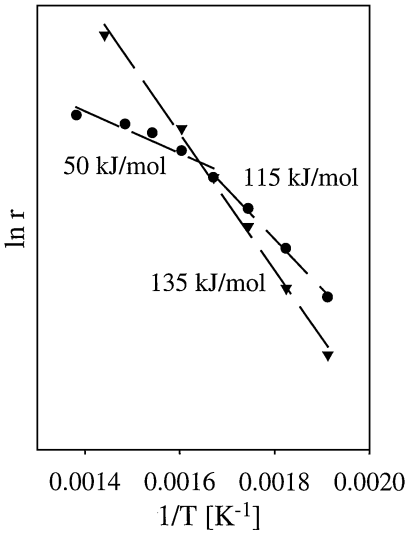

FIG. 10. Arrhenius plots of the n-heptane hydroconversion over 1 wt% Pd/SAPO-11/4 (●) and 1 wt% Pd/SAPO-5 (▼): $p = 3$ bar; $p_{C_7} = 25$ mbar.

Over both SAPO-11 and SAPO-5 methylhexanes are the only reaction products obtained at low conversions. Conversion yield curves clearly show that isomerization and cracking of *n*-heptane are consecutive reactions, as expected from the bifunctional mechanism (1, 38). High amounts of methyl isomers with a preference to 2-MC_6 over SAPO-11 and to 3-MC_6 over SAPO-5 were detected. Among the dimethylpentanes, the formation of 2,3-DMC_5 is greatly favored. The isobutane/*n*-butane ratio, being much higher on SAPO-5 than on SAPO-11, indicates that over large pore SAPO-5 multibranched isomers can be formed, which are rapidly cracked via ß-scission.

The preferential formation of 2-MC_6 over SAPO-11 was attributed to restricted transition-state shape selectivity (40). In the narrow channels the constraint exerted by the limited space in the pores has a significant influence on the formation of the PCP intermediates. The approximate size of the cyclopropane ring is 0.43 nm which can be accommodated within the pore of SAPO-11. It was suggested that PCP intermediates with the ring at the terminal position are less rigid than the PCP with the ring in internal positions and thus the most favored according to the restricted transition state shape selectivity. Mériaudeau *et al.* (9) suggested that the high selectivity to terminally branched isomers is a result of restricted transition state selectivity at the pore mouth of the channels. But the increase of activity and isomerization selectivity with increasing concentration of acid sites reported here indicates that the reaction products are presumably formed within the channels. Thus, product diffusion and shape selectivity also contribute to the overall selectivity in methyl branching reactions. The somewhat lower activity in the *n*-C_7 conversion observed for the SAPO-11 samples synthesized with aluminum isopropoxide (see Fig. 6) could be caused by the formation of spherical aggregates (Fig. 2c) which can induce a restricted accessibility to the pores.

Conversion of Monobranched Isomers

2-MC_6 and 3-MC_6 have several reaction possibilities to produce primary products: (i) methyl shift, (ii) branching to ethyl- and dimethyl-C_5, (iii) unbranching to *n*-C_7, and (iv) type C ß-scission to propane and *n*-butane. It is well established for carbenium ion rearrangements that reactions, where the degree of branching does not change, are 4 to 5 times faster than PCP branching or unbranching reactions and much faster than ß-cracking (41). It seems therefore to be reasonable that 3-MC_6/2-MC_6 is the most abundant reaction product of the 2-MC_6/3-MC_6 conversion over SAPO-5 and SAPO-11.

In the larger pore system of SAPO-5, dibranched isomers with the thermodynamically favored 2,3-DMC_5 as the main product prevail beside the monobranched isomers (Table 4a), whereas in the narrow pore system of SAPO-11 the amount of *n*-C_7 formed was about 6 times higher than the amount of dibranched isomers. This difference in unbranching to *n*-C_7 between SAPO-5 and SAPO-11 confirms the assumption that reactions occur inside the pores.

The activation energies for the 2-MC_6 conversion were almost identical to that of the *n*-C_7 conversion. The higher rate for 2-MC_6 over SAPO-5 and SAPO-11 in comparison to the conversion of *n*-C_7 can be explained by a larger number of possible reaction pathways, including the 1,2-methyl shift as a very fast reaction. In addition, the diffusion coefficients of 2-MC_6 and *n*-C_7 possess nearly the same value, being even greater for 2-MC_6 in SAPO-11. The apparent activation energy for 3-MC_6 was lower than that for 2-MC_6, reflecting the lower diffusivity of 3-MC_6.

Conversion of Dibranched Isomers

Primary products from the conversion of dibranched heptane isomers result from a methyl shift, from further branching or unbranching to monomethyl-isomers, and from ß-scission to cracked products. 2,3-DMC_5 was the main product from the isomerization of 2,4-DMC_5 over SAPO-5 and SAPO-11. In the large pore SAPO-5, the dibranched isomers prevail, whereas monomethyl-C_6 and even *n*-C_7 were found over SAPO-11. The rate constants given (41) for alkylcarbenium ion rearrangements suggest that the 1,2-methyl shift was about 100 times faster than mono- to *n*-unbranching reactions. However, due to the longer residence time in the smaller pores of SAPO-11 and the tendency to form products that are mobile inside the pores, the latter reaction could be favored.

By ir spectroscopy it was shown that the diffusion coefficients and the number of accessible acid sites for 2,4-DMC_5 are close to those of 2,3-DMC_5, which is also reflected in comparable activity of both molecules over both SAPO-5 and −11.

Over SAPO-5 the main products from the conversion of 2,3-DMC_5 are 2,2-, 3,3-, and 2,4-DMC_5. The isomer distribution obtained from 2,4-DMC_5, where less 2,2- and 3,3-DMC_5 was formed compared to the 2,3-DMC_5, indicates a preference for a methyl shift to a neighboring C atom. These bulky isomers are only detected in small concentrations over SAPO-11 where preferentially unbranching to monomethyl isomers and *n*-C_7 occurs.

The lower rate for the conversion of dibranched isomers on SAPO-11 can be explained by a restricted availability of acid sites and diffusion limitation. However, the decrease in the rate is less significant as in the case of 10-membered zeolites such as HZSM-5 (42).

In general, the intracrystalline surface is almost 2 orders of magnitude larger than the external surface. In the absence of diffusion limitation the contribution of the outer surface is negligible. When the molecule is too large to enter the pores, the internal surface will not contribute to the overall catalytic activity. Mériaudeau *et al.* (26) found higher

activity in *n*-alkane hydroconversion over small crystals of SAPO-11 than over large crystals and they discussed this behavior in terms of pore mouth catalysis. But if the reaction took place only at the pore mouths of the catalyst, the same or an even higher activity of the dibranched molecules compared to linear or monobranched molecules could be expected on SAPO-11.

Conversion of the Tribranched Isomer

2,2,3-TMC_4 as a reactant is only interacting with the outer surface of the SAPO-11 catalyst, whereas it is still able to enter the pores of SAPO-5. The reactivity of this molecule is rather low. The first step must be unbranching to dimethylpentanes that can react further by a methyl shift, unbranching, and cracking. The apparent activation energies indicated that the reaction is strongly diffusion limited, even over SAPO-5.

CONCLUSIONS

A series of Pd-impregnated SAPO-11 (with different acid site concentrations but with the same acid strength) and one SAPO-5 with a somewhat lower acid strength were used as catalysts in the hydroconversion of heptane isomers.

The activity in *n*-heptane conversion increases until a Pd/acid site ratio of 0.02–0.03 is reached. An increasing concentration of acid sites results in an enhancement of the activity and the isomerization selectivity, showing that hydroconversion over the different Pd–SAPO-11 samples must essentially be governed by acidity.

It was shown that the Brønsted acid sites in SAPO-11 and in SAPO-5 are completely accessible at 10^{-3} mbar for n-C_7 and 2-MC_6. The influence of the n-C_7 and 2-MC_6 transport inside the pores is negligible at low temperatures and low conversions. Severe diffusion limitations for the multibranched isomers and an interaction with the bridged acid sites of 20% with 2,3- and 2,4-DMC_5 and of about 5% with 2,2,3-TMC_4 at an equilibrium pressure of 1 mbar were found in SAPO-11. All acid sites in SAPO-5 are accessible for the dibranched isomers but the diffusion coefficients were smaller compared to those of n-C_7 and 2-MC_6. Differences in the pore dimensions of SAPO-5 and SAPO-11 and thus in the diffusion coefficients are reflected in the different reactivities and in the product distributions of the heptane isomers.

The Pd-particle size estimated from the metal dispersion was between 15 and 30 nm, suggesting that the particles are too large to fit into the SAPO pores.

For hybrid catalysts consisting of Pd/SiO_2 and SAPO-11 almost the same activity and selectivity in *n*-heptane conversion was found as those for impregnated SAPO-11, indicating that the distance between acid and metal sites has only a minor influence, as long as the supported metal and the SAPO phase are in direct contact.

ACKNOWLEDGMENTS

We gratefully acknowledge the financial support of this work by the "Fond zur Förderung der wissenschaftlichen Forschung," Project No. 11749, and the "Oesterreichische Nationalbank" Project No. 5410.

REFERENCES

1. Campelo, J. M., Lafont, F., and Marinas, J. M., *J. Catal.* **156**, 11 (1995).
2. Parlitz, B., Schreier, E., Zubowa, H. L., Eckelt, R., Lieske, E., Lischke, G., and Fricke, R., *J. Catal.* **155**, 1 (1995).
3. Chaar, M. A., and Butt, J. B., *Appl. Catal. A* **114**, 287 (1994).
4. Sinha, A. K., and Sivasanker, S., *Catal. Today* **49**, 293 (1999).
5. Miller, S. J., U.S. Patent 5,149,421, 1992.
6. Miller, S. J., *Microporous Mater.* **2**, 439 (1994).
7. Jacobs, P. A., Martens, J. A., Weitkamp, J., and Beyer, H. K., *Faraday Discuss. Chem. Soc.* **72**, 353 (1982).
8. Martens, J. A., and Jacobs, P. A., *Zeolites* **6**, 334 (1986).
9. Mériaudeau, P., Tuan, V. A., Lefebvre, F., Nghiem, V. T., and Naccache, C., *Microporous Mesoporous Mater.* **22**, 435 (1998).
10. Chen, N. Y., Degnan, T. F., and Smith, C. M., "Molecular Transport and Reaction in Zeolites," pp. 131 ff. VCH Publishers, New York, 1994.
11. Weisz, P. B., and Swegler, E. W., *Science* **126**, 31 (1957).
12. Tiong Sie, S., *Ind. Eng. Chem. Res.* **31**, 1881 (1992).
13. Tiong Sie, S., *Ind. Eng. Chem. Res.* **32**, 397 (1993).
14. Tiong Sie, S., *Ind. Eng. Chem. Res.* **32**, 403 (1993).
15. Yue Chu, H., Rosynek, M. P., and Lunsford, J. H., *J. Catal.* **178**, 352 (1998).
16. Iglesia, E., Soled, S. L., and Kramer, G. M., *J. Catal.* **144**, 238 (1993).
17. Zhang, A., Nakamura, I., Aimoto, K., and Fujimoto, K., *Ind. Eng. Chem. Res.* **34**, 1074 (1995).
18. McCarthy, T. J., Lei, G.-D., and Sachtler, W. M. H., *J. Catal.* **159**, 90 (1996).
19. Lok, B. M., Messina, C. A., Patton, R. L., Gajek, R. T., Cannan, T. R., and Flanigen, E. M., U.S. Patent 4,440,871, 1984.
20. Höchtl, M., Jentys, A., and Vinek, H., *in* "Porous Materials in Environmentally Friendly Processes" (I. Kiricsi, G. Pál-Borbély, J. B. Nagy, and H. G. Karge, Eds.), Studies Surface Science and Catalysis, Vol. 125, p. 425. Elsevier, Amsterdam, 1999.
21. Tapp, N. J., Milestone, N. B., and Bibby, D. M., *Zeolites* **8**, 183 (1988).
22. Benson, J. E., Hwang, H. S., and Boudart, M., *J. Catal.* **30**, 146 (1973).
23. Höchtl, M., Jentys, A., and Vinek, H., *Microporous Mesoporous Mater.* **31**, 271 (1999).
24. Breck, D. W., "Zeolite Molecular Sieves," p. 636. Wiley-Interscience, New York, 1974.
25. J. Crank, "Mathematics of Diffusion," pp. 62 ff. Oxford University Press, London, 1956.
26. Mériaudeau, P., Tuan, V. A., Nghiem, V. T., Lai, S. Y., Hung, L. N., and Naccache, C., *J. Catal.* **169**, 55 (1997).
27. Alberty, R. A., and Gehrig, C. A., *J. Phys. Chem. Ref. Data* **13**, 1173 (1984).
28. Mertens, M., Martens, J. A., Grobet, P. J., and Jacobs, P. A., *in* "Guidelines for Mastering the Properties of Molecular Sieves" (D. Barthomeuf, E. Derouane, and W. Hölderich, Eds.), p. 1. Plenum Press, New York, 1990.
29. Meier, W. M., Olson, D. H., and Baerlocher, Ch., *Zeolites* **17**, 20 (1996).
30. Voogd, P., and van Bekkum, H., *in* "Zeolites as Catalysts, Sorbents and Detergent Builders" (H. G. Karge and J. Weitkamp, Eds.), Studies Surface Science and Catalysis, Vol. 46, p. 585. Elsevier, Amsterdam, 1989.
31. Webb, E. B., III, and Grest, G. S., *Catal. Lett.* **56**, 95 (1998).

32. Höchtl, M., and Vinek, H., unpublished experimental results.
33. Guisnet, M., Alvarez, F., Giannetto, G., and Perot, G., *Catal. Today* **1**, 415 (1987).
34. Bai, X., and Sachtler, W. M. H., *J. Catal.* **129**, 121 (1990).
35. Van de Runstraat, A., Van Grondelle, J., and Van Santen, R. A., *Ind. Eng. Chem. Res.* **36**, 3116 (1997).
36. Baumgarten, E., Lentes-Wagner, C., and Wagner, R., *J. Catal.* **117**, 533 (1989).
37. Paál, Z., Räth, M., Zhan, Z., and Gombler, W., *J. Catal.* **147**, 342 (1994).
38. M. Höchtl, Thesis, University of Technology, Vienna, Austria, 1999.
39. Eder, F., Thesis, University of Twente, Enschede, The Netherlands, 1996.
40. Ernst, S., Weitkamp, J., Martens, J. A., and Jacobs, P. A., *Appl. Catal. A* **48**, 137 (1989).
41. Martens, J. A., and Jacobs, P. A., *in* "Theoretical Aspects of Heterogeneous Catalysis" (J. B. Moffat, Ed.), p. 69. Van Nostrand Reinhold, New York, 1990.
42. Weisz, P. B., *Pure Appl. Chem.* **52**, 2091 (1980).